Scientific Research Publishing

Journal of Applied Mathematics and Physics, 2025, 13(9), 2976-2990
https://www.scirp.org/journal/jamp
ISSN Online: 2327-4379
ISSN Print: 2327-4352

The Rectangular 2D Cartesian Plane Framework of Curve Functions Involving Radius of Curvature—Nonlinear Differential Equations with Application to Regular Wedge Cam Design

Shawn P. Guillory

Department of Mechanical Engineering, The University of Louisiana at Lafayette, Lafayette, LA, USA
Email: shawn.guillory1@louisiana.edu

How to cite this paper: Guillory, S.P. (2025) The Rectangular 2D Cartesian Plane Framework of Curve Functions Involving Radius of Curvature—Nonlinear Differential Equations with Application to Regular Wedge Cam Design. *Journal of Applied Mathematics and Physics*, **13**, 2976-2990.
https://doi.org/10.4236/jamp.2025.139170

Received: August 13, 2025
Accepted: September 15, 2025
Published: September 18, 2025

Abstract

In the study of radius of curvature differential equations, a generalized closed-form analytical solution to the curve function $y(x)$ in a rectangular 2D Cartesian plane is determined under the assumption that the radius of curvature function and initial conditions are known, specified quantities. Various mathematical examples are provided to demonstrate the validity of the differential equation solution. A more comprehensive application is then shown regarding a regular wedge cam mechanism design associated with three-point self-centering motion for its potential use when optimizing cam characteristics and associated machinery design related to curvature.

Keywords

Radius of Curvature, Differential Equation, Simpson's Rule, Three-Point Self-Centering Motion, Regular Wedge Cam Design, Design Optimization

1. Introduction

The study of curvature in geometry and its relationship with differential equations is a central topic in both pure and applied mathematics. One of the fundamental measures in the analysis of curves is the radius of curvature, which quantifies how sharply a curve bends at a given point. Understanding and calculating the radius of curvature plays an important role in various fields, such as mechanics, physics, computer graphics, and engineering. Analytical solutions to the differential equa-

tions governing the radius of curvature are vital in many contexts, providing a more precise understanding of the behavior of curves in different systems.

Finding analytical solutions to the differential equations governing the radius of curvature can be challenging, especially when the curve is defined by non-trivial functions. In many cases, solving these equations requires advanced calculus methods, including integration and series expansions. For example, for simple curves such as parabolas or circles, exact solutions for the radius of curvature are relatively straightforward. However, numerical methods or approximation techniques are often employed for more complex curves, such as those governed by transcendental functions.

Further details regarding its application uses are discussed. In mechanics, the radius of curvature is essential for analyzing the motion of particles and rigid bodies. The force exerted on an object moving along a curved path, such as a car on a road, depends on the radius of curvature, as it directly influences the acceleration due to centripetal force. Analytical expressions for the radius of curvature allow engineers to calculate the forces acting on objects in curved motion [1].

Additionally, in structural engineering, the radius of curvature is used to analyze the behavior of beams and arches. The curvature of structural elements affects the distribution of stress and strain, and understanding these effects is vital for designing safe and efficient structures. For example, the bending of beams can be modeled using the relationship between curvature and applied loads, where the radius of curvature varies with position along the beam [2]. By solving the corresponding differential equations, which may be as much as fourth-order Euler-Bernoulli PDEs, engineers can determine the stresses in structures under bending.

Furthermore, in computer graphics and geometric modeling, the radius of curvature is used in the design of smooth curves and surfaces, particularly in applications involving Computer-Aided Design (CAD) and animation. Curves such as Bézier curves and B-splines are often used to model smooth shapes, where the radius of curvature is critical for ensuring the smoothness and visual appeal of the modeled object [3]. In such applications, analytical solutions are often employed to ensure that the radius of curvature meets certain aesthetic or functional criteria.

Moreover, in robotics, particularly in motion planning, the radius of curvature plays an important role in path planning and trajectory design. Robots are required to follow smooth and efficient paths that avoid obstacles while minimizing energy consumption or time. Analytical and numerical methods to compute the radius of curvature are essential for designing these paths, ensuring that the robot follows a trajectory that is both feasible and efficient [4].

Despite the importance of the radius of curvature in various fields, challenges remain in finding exact analytical solutions for complex curves. In particular, curves described by high-degree polynomials or transcendental functions often do not have simple closed-form solutions, making numerical methods indispensable. As computational power continues to grow, the development of more efficient numerical methods, such as Finite Element Analysis (FEA) and computa-

tional geometry techniques, is expected to lead to further advances in the accuracy and applicability of curvature analysis in real-world problems [5].

As such, we examine the radius of curvature in differential equation form, specifically for general curves in the rectangular 2D Cartesian plane framework. A general closed-form curve function solution for all possible curves in this framework is determined by solving the associated nonlinear second-order nonhomogeneous ordinary differential equation. However, there are some cases where Simpson's rule may be used to determine the singular and/or nested integrals. Nevertheless, each curve can be found successfully by using the provided exact general solution and Simpson's equations, which eliminates the common requirement for different methods or approaches to find the curve solution analytically. In summary, we present: 1) a fully generalized closed-form analytical solution, 2) antiderivative approximations by Simpson's rule, 3) mathematical validation examples with semicircles, parabolas, and transcendental functions, and 4) application to a self-centering regular wedge cam contour solution in rectangular form based on the radius of curvature.

2. Methodology

2.1. Generalized Closed-Form Analytical Curve Function Solution

For a curve $y(x)$ in the rectangular 2D Cartesian plane, the radius of curvature $r_{rc}(x)$ of a circle that best approximates the curve at any point can be defined by:

$$r_{rc}(x)=\frac{\left(1+y'(x)^2\right)^{3/2}}{y''(x)}, \tag{1}$$

where $y'(x)$ is the first derivative (slope) and $y''(x)$ is the second derivative (curvature) [6]. This formula provides an explicit relationship between the geometry of the curve and its curvature.

For other types of curves, such as those described parametrically or in multiple dimensions, the formula for $r_{rc}(x)$ can be extended to account for the general form of the curve [7]. The radius of curvature for more complex curves, such as space curves or those in multiple dimensions, is defined through the Frenet-Serret formulas, which describe the behavior of the tangent vector, normal vector, and binormal vector along the curve [8]. These formulas yield a system of differential equations that can be solved to obtain the radius of curvature in higher-dimensional settings [9].

Moreover, the radius of curvature is a fundamental concept that arises naturally in differential geometry, where the curvature of a curve $\kappa(x)$ is defined as the reciprocal of the radius ($1/r_{rc}(x)$) to measure the convergence/divergence of the approximate circle from the actual curve. In this research, the area under the curvature's curve in variation with the spatial coordinate x will be used and is denoted as $A_\kappa(x)$.

$$A_\kappa(x)=\int \kappa(x)\mathrm{d}x \tag{2}$$

Under the assumption that the radius of curvature is known, Equation (1) is an Ordinary Differential Equation (ODE), where $y(x)$ is an unknown curve function. Due to the ODE's structure, it is classified as nonlinear, second order, and nonhomogeneous. Therefore, a suitable set of initial conditions comprised of the initial path point $y(x_0)=y_0$ and the slope at this point $y'(x_0)=m_0$ is employed for constructing a fully generalized closed-form analytical ODE solution $y(x)$ for any known/specified radius of curvature function.

The solution to Equation (1) is presented as follows where $\lambda(x)$ is a quantity that determines whether the solution is real or complex, $U(x)$ is the integrand of $\epsilon(x)$, c_1 and c_2 are constants of integration, $y(x)$ is the ODE solution, and $y'(x)$ and $y''(x)$ are successive derivatives of the ODE solution. Furthermore, the initial slope condition value m_0 is used in conjunction with Equation (9) to obtain the equation for c_1, and the initial path condition value is combined with Equation (8) to obtain the equation for c_2. To note, since there are multiple curve solutions that may satisfy both the initial conditions and the specified radius of curvature equation, parameters s_1 and s_2 are utilized to denote plus/minus fluctuations that account for the four possible curve solution constructs.

$$\lambda(x) = 1 - c_1^2 - 2\,c_1 A_\kappa(x) - A_\kappa^2(x) \tag{3}$$

$$U(x) = \frac{c_1 + A_\kappa(x)}{\sqrt{\lambda(x)}} \tag{4}$$

$$\epsilon(x) = \int U(x)\,\mathrm{d}x \tag{5}$$

$$c_1 = s_2 \frac{\sqrt{m_0^2 + m_0^4}}{1 + m_0^2} - A_\kappa(x_0) \tag{6}$$

$$c_2 = y_0 - s_1 \epsilon(x_0) \tag{7}$$

$$y(x) = c_2 + s_1 \epsilon(x) \tag{8}$$

$$y'(x) = s_1 U(x) \tag{9}$$

$$y''(x) = \frac{s_1}{r_{rc}(x)}\left(\frac{(c_1 + A_\kappa(x))^2}{\lambda(x)^{3/2}} + \frac{1}{\sqrt{\lambda(x)}}\right) \tag{10}$$

2.2. Antiderivative Approximations by Simpson's Rule

For some cases of radius of curvature, antiderivative solutions to the integrals involved with the ODE solution and its successive derivatives are difficult (even for computer programs) to determine analytically. Therefore, antiderivative approximations as per Simpson's rule (relying on left and right Riemann sums, the midpoint rule, and the trapezoid rule) are applied to the integrals seen in Equations (2) and (5) [10]. However and prior to presenting the previously mentioned approximations, the indefinite integrals are converted into definite integral forms, specifically from x_0 to x, for approximation requirements and to simplify the constants of integration.

$$A_\kappa(x) = \int_{x_0}^{x} \kappa(x)\,\mathrm{d}x \tag{11}$$

$$\in(x)=\int_{x_0}^{x}U(x)\mathrm{d}x \tag{12}$$

$$c_1=s_2\frac{\sqrt{m_0^2+m_0^4}}{1+m_0^2} \tag{13}$$

$$c_2=y_0 \tag{14}$$

Since Equation (11) has only one integral, it can be approximated by Equations (16) to (20) (varying in accuracy levels) where h_1 is the step size equation, and parameter n is the number of subdivisions used to obtain the desired accuracy level. To note, Equation (20) is the final, most accurate Simpson's rule approximation which relies on all previous approximations.

$$h_1(x)=\frac{x-x_0}{n} \tag{15}$$

$$A_{\kappa L_1}(x)=LEFT_1(x)=\sum_{i=0}^{n-1}\kappa\left(x_0+ih_1(x)\right)h_1(x) \tag{16}$$

$$A_{\kappa R_1}(x)=RIGHT_1(x)=\sum_{i=1}^{n}\kappa\left(x_0+ih_1(x)\right)h_1(x) \tag{17}$$

$$A_{\kappa M_1}(x)=MID_1(x)=\sum_{i=0}^{n-1}\kappa\left(x_0+ih_1(x)+\frac{h_1(x)}{2}\right)h_1(x) \tag{18}$$

$$A_{\kappa T_1}(x)=TRAP_1(x)=\frac{A_{\kappa L_1}(x)+A_{\kappa R_1}(x)}{2} \tag{19}$$

$$A_{\kappa S_1}(x)=SIMP_1(x)=\frac{2A_{\kappa M_1}(x)+A_{\kappa T_1}(x)}{3} \tag{20}$$

The approximation of Equation (12) is more complicated since it contains integrals of curvature nested within the outermost integral. To accomplish this, the approximations provided by Equations (22) to (26) are rewritten from above based on a new step size equation h_2 and index parameter j, where m is the number of subdivisions used only for the integral of curvature (which is nested inside the outermost integral).

$$h_2(x)=\frac{ih_1(x)-x_0}{m} \tag{21}$$

$$A_{\kappa L_2}(x)=LEFT_2(x)=\sum_{j=0}^{m-1}\kappa\left(x_0+jh_2(x)\right)h_2(x) \tag{22}$$

$$A_{\kappa R_2}(x)=RIGHT_2(x)=\sum_{j=1}^{m}\kappa\left(x_0+jh_2(x)\right)h_2(x) \tag{23}$$

$$A_{\kappa M_2}(x)=MID_2(x)=\sum_{j=0}^{m-1}\kappa\left(x_0+jh_2(x)+\frac{h_2(x)}{2}\right)h_2(x) \tag{24}$$

$$A_{\kappa T_2}(x)=TRAP_2(x)=\frac{A_{\kappa L_2}(x)+A_{\kappa R_2}(x)}{2} \tag{25}$$

$$A_{\kappa S_2}(x)=SIMP_2(x)=\frac{2A_{\kappa M_2}(x)+A_{\kappa T_2}(x)}{3} \tag{26}$$

Combined with Equations (22) to (26), the complete approximation of $\epsilon(x)$ is defined as follows, where the index parameter for the *outermost* integral is i, its number of subdivisions is n, and, therefore, its step size is h_1. Note that while the equations for $U(x)$ with subscripts *L*, *R*, and *M* were not defined directly, they can be obtained by using Equation (4) in conjunction with Equations (3) and (22) to (26).

$$\epsilon_L(x) = LEFT_3(x) = \sum_{i=0}^{n-1} U_L\left(x_0 + ih_1(x)\right)h_1(x) \tag{27}$$

$$\epsilon_R(x) = RIGHT_3(x) = \sum_{i=1}^{n} U_R\left(x_0 + ih_1(x)\right)h_1(x) \tag{28}$$

$$\epsilon_M(x) = MID_3(x) = \sum_{i=0}^{n-1} U_M\left(x_0 + ih_1(x) + \frac{h_1(x)}{2}\right)h_1(x) \tag{29}$$

$$\epsilon_T(x) = TRAP_3(x) = \frac{\epsilon_L(x) + \epsilon_R(x)}{2} \tag{30}$$

$$\epsilon_S(x) = SIMP_3(x) = \frac{2\epsilon_M(x) + \epsilon_T(x)}{3} \tag{31}$$

3. Results with Results Discussion

3.1. The Semicircles Validation Example

Validation of the nonlinear radius of curvature differential equation theory is shown with a constant radius of curvature ($r_{rc}(x) = 2$). It is known that a circular path (which is comprised of two semicircle functions) is associated with a constant radius of curvature. The initial conditions presented below (at $x_0 = 0$) are expected to produce a positive semicircle ($y(x) = \sqrt{4 - x^2}$).

$$y(x_0) = 2 \quad \text{and} \quad y'(x_0) = 0 \tag{32}$$

The exact equations of nonlinear ODE theory, with all values for s_1 and s_2, shows that the combined curve solution and successive derivatives are:

$$y(x) = 2 \pm \left(2 - \sqrt{4 - x^2}\right), \tag{33}$$

$$y'(x) = \pm \frac{x}{\sqrt{4 - x^2}}, \tag{34}$$

$$y''(x) = \pm \frac{r^2}{\left(4 - x^2\right)^{3/2}}. \tag{35}$$

The radius of curvature that results from these equations result in $r_{rc} = \pm 2$, (which is plus/minus the specified radius of curvature equation). This is not an issue due to the concept of radius of curvature, and, therefore, validates the differential equation theory. The combined graph(s) associated with the curve solution and successive derivatives are given in Figure 1 below to demonstrate the nature of the example solution.

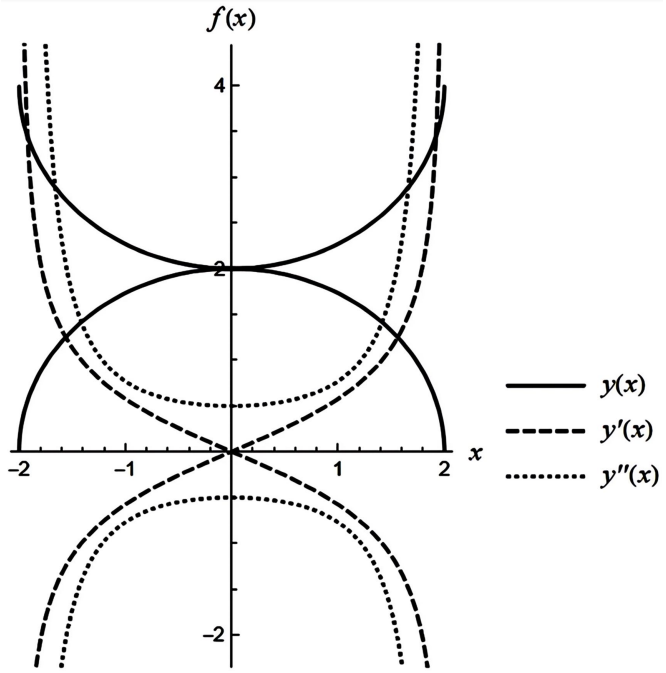

Figure 1. Example 1 graph of circle ODE solution and its successive derivatives.

3.2. The Parabolas Validation Example

Further validation of the nonlinear radius of curvature differential equation theory is shown with a radius of curvature that corresponds to a simple parabolic curve ($y(x)=x^2$). The initial conditions presented below (at $x_0=0$) are expected to produce a parabolic curve with its vertex coincident with the origin of the Cartesian plane.

$$r_{rc}(x)=\frac{1}{2}\left(1+4x^2\right)^{3/2} \tag{36}$$

$$y(x_0)=0 \quad \text{and} \quad y'(x_0)=0 \tag{37}$$

The exact equations of nonlinear ODE theory, with all values for s_1 and s_2, shows that the combined curve solution and successive derivatives are:

$$y(x)=\pm x^2, \tag{38}$$

$$y'(x)=\pm 2x, \tag{39}$$

$$y''(x)=\pm 2. \tag{40}$$

The radius of curvature that arises from these equations is:

$$r_{rc}(x)=\pm\frac{1}{2}\left(1+4x^2\right)^{3/2}, \tag{41}$$

(Which is plus/minus the specified radius of curvature equation). This is not an issue due to the concept of radius of curvature, and therefore, validates the differential equation theory. The combined graph(s) associated with the curve solution and successive derivatives is given in Figure 2 below to demonstrate the nature of the example solution.

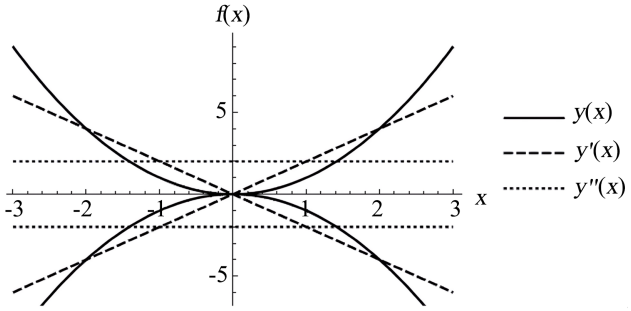

Figure 2. Example 2 graph of parabolic ODE solution and its successive derivatives.

3.3. The Transcendental Functions Validation Example

Further validation of the nonlinear radius of curvature differential equation theory is shown with a radius of curvature that obeys the transcendental function defined by Equation (42). The initial conditions presented below (at $x_0 = 0$) are arbitrarily prescribed to provide insight into what kind of curve function solutions are obtained.

$$r_{rc}(x) = \frac{\sin 2x}{\sin 4x}(1+\sin 2x)^{3/2} \tag{42}$$

$$y(x_0) = 1 \quad \text{and} \quad y'(x_0) = 0 \tag{43}$$

Exact equations of nonlinear ODE theory regarding $r_{rc}(x)$, with all values for s_1 and s_2, show that the combined curve solution and successive derivatives are:

$$y(x) = 1 \pm \frac{1}{2}(1-\cos 2x), \tag{44}$$

$$y'(x) = \pm \sin 2x, \tag{45}$$

$$y''(x) = \pm 2\cos 2x. \tag{46}$$

The radius of curvature that arises from these equations result in:

$$r_{rc}(x) = \pm \frac{(1+\sin 2x)^{3/2}}{\cos 2x} \equiv \pm \frac{\sin 2x}{\sin 4x}(1+\sin 2x)^{3/2} \tag{47}$$

(which is plus/minus the specified radius of curvature equation). This is not an issue due to the concept of radius of curvature, and therefore, validates the differential equation theory. The combined graph(s) associated with the curve solution and successive derivatives is given in **Figure 3** below to demonstrate the nature of the example solution.

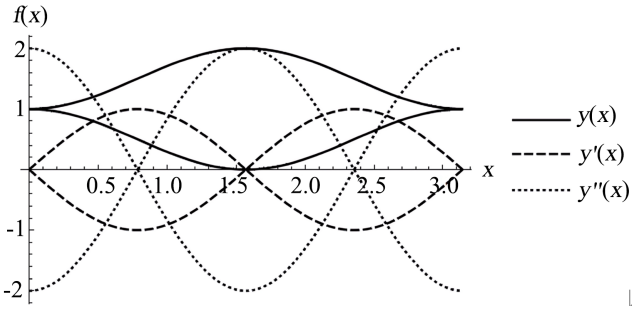

Figure 3. Example 3 graph of transcendental ODE solution and its successive derivatives.

3.4. The Three-Point Self-Centering Regular Wedge Cam Design Application with Numerical Validation

The application process involving the nonlinear radius of curvature differential equation theory shown through this example occurs when the radius of curvature and initial conditions are determined in context of a three-point self-centering regular wedge cam mechanism design type. To note, the radius of curvature is determined parametrically in conjunction with an exact backward kinematic cam rotation solution $\theta(x_{cr})$ determined from a developed trigonometric substitution & transformation (TS&T) method [11].

To accomplish this, various equations are used to define the parametric regular wedge cam contour transformation equations, $x_{cr}(\theta)$ and $y_{cr}(\theta)$ (in accordance with **Figure 4**), as well as the path's end point—as per the maximum cam angle θ_{max}. Note that the specified/driving analysis variables necessary for all related equations regarding the regular cam design are R_{wmax}, R_{wmin}, r, C_{lrx}, φ_o, x_1, y_1, x_2, and y_2 [11].

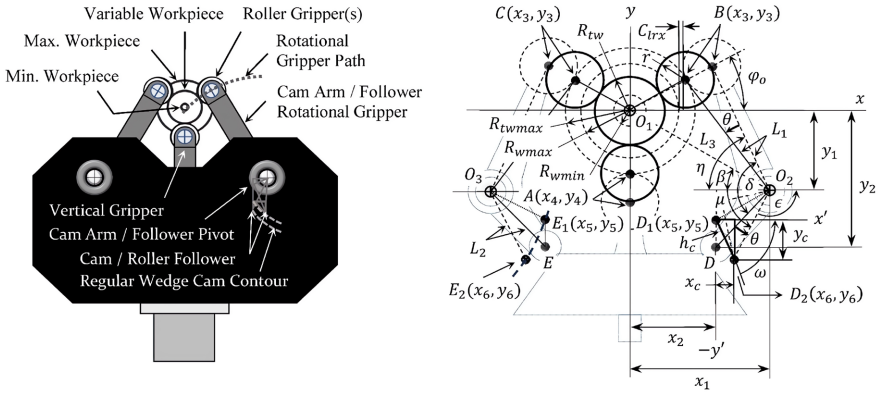

Figure 4. The kinematic self-centering regular wedge cam motion layout.

The associated driven/fixed analysis variables are defined as:

$$R_{twmax} = \frac{R_{wmax} + C_{lrx} + r}{\cos\varphi_o} - r, \tag{48}$$

$$L_1 = \sqrt{\left(x_1 - \left(R_{twmax} + r\right)\cos\varphi_o\right)^2 + \left(y_1 + \left(R_{twmax} + r\right)\sin\varphi_o\right)^2}, \tag{49}$$

$$L_3 = \sqrt{x_1^2 + y_1^2}, \tag{50}$$

$$\eta = \frac{\pi}{2} - \tan^{-1}\frac{x_1 - \left(R_{twmax} + r\right)\cos\varphi_o}{y_1 + \left(R_{twmax} + r\right)\sin\varphi_o}, \tag{51}$$

$$\beta = \tan^{-1}\frac{y_1}{x_1}. \tag{52}$$

Several variable coordinate point equations involved with the regular wedge cam equations are described as follows.

$$\begin{aligned} x_3(\theta) = x_1 &- \left(x_1 - \left(R_{twmax} + r\right)\cos\varphi_o\right)\cos\theta \\ &- \left(y_1 + \left(R_{twmax} + r\right)\sin\varphi_o\right)\sin\theta \end{aligned} \tag{53}$$

$$y_3(\theta) = -y_1 - \left(x_1 - \left(R_{twmax} + r\right)\cos\varphi_o\right)\sin\theta + \left(y_1 + \left(R_{twmax} + r\right)\sin\varphi_o\right)\cos\theta \tag{54}$$

$$R_{tw}(\theta) = \sqrt{x_3^2(\theta) + y_3^2(\theta)} - r \tag{55}$$

$$x_5 = x_2 \tag{56}$$

$$y_5(\theta) = y_2 - \left(R_{twmax} - R_{tw}(\theta)\right) \tag{57}$$

$$x_6(\theta) = x_1 + \left(x_2 - x_1\right)\cos\theta + \left(y_2 - y_1\right)\sin\theta \tag{58}$$

$$y_6(\theta) = y_1 - \left(x_2 - x_1\right)\sin\theta + \left(y_2 - y_1\right)\cos\theta \tag{59}$$

The resulting parametric transformation regular wedge cam path equations and the maximum cam angle that terminates the end point of the cam path are expressed as:

$$x_{c_r}(\theta) = x_6(\theta) - x_2, \tag{60}$$

$$y_{c_r}(\theta) = y_6(\theta) - y_5(\theta), \tag{61}$$

$$\theta_{max} = \eta - \beta - \cos^{-1}\frac{L_1^2 + L_3^2 - \left(r + R_{wmin}\right)^2}{2L_1L_3}. \tag{62}$$

The associated backward kinematic cam rotation equations based on TS&T are:

$$\Theta\left(x_{c_r}\right) = \frac{y_1 - y_2}{2\left(x_1 - x_2\right) - x_{c_r}} \pm \frac{\sqrt{2\left(\left(x_1 - x_2\right)x_{c_r} - y_1y_2\right) - x_{c_r}^2 + y_1^2 + y_2^2}}{2\left(x_1 - x_2\right) - x_{c_r}}, \tag{63}$$

$$\theta\left(x_{cr}\right) = 2\tan^{-1}\Theta\left(x_{c_r}\right). \tag{64}$$

Furthermore, the successive spatial derivatives of the parametric cam equations are defined below (by Equations (74) to (77)), where a and b are amplitudes of the wave equations $c_w(\theta)$. These wave equations are used in conjunction with the vertical coordinate point $y_4(\theta)$ of the roller's center point A as previously shown in **Figure 4**.

$$a_{1_r} = 2y_1\left(x_1 - \left(R_{twmax} + r\right)\cos\varphi_o\right) \tag{65}$$

$$b_{1_r} = 2x_1\left(x_1 - \left(R_{twmax} + r\right)\cos\varphi_o\right) \tag{66}$$

$$a_{2_r} = -2x_1\left(y_1 + \left(R_{twmax} + r\right)\sin\varphi_o\right) \tag{67}$$

$$b_{2_r} = 2y_1\left(y_1 + R_{twmax} + r\right)\sin\varphi_o) \tag{68}$$

$$c_{w_{1_r}}(\theta) = a_{1_r}\cos\theta + b_{1_r}\sin\theta \tag{69}$$

$$c_{w_{2_r}}(\theta) = a_{2_r}\cos\theta + b_{2_r}\sin\theta \tag{70}$$

$$c_{w_{3_r}}(\theta) = b_{1_r}\cos\theta - a_{1_r}\sin\theta \tag{71}$$

$$c_{w_{4_r}}(\theta) = b_{2_r}\cos\theta - a_{2_r}\sin\theta \tag{72}$$

$$y_4(\theta) = R_{tw}(\theta) + r \tag{73}$$

$$x'_{c_r}(\theta) = \frac{\mathrm{d}x_{c_r}(\theta)}{\mathrm{d}\theta} = \left(y_2 - y_1\right)\cos\theta - \left(x_2 - x_1\right)\sin\theta \tag{74}$$

$$x''_{c_r}(\theta)=\frac{\mathrm{d}^2x_{c_r}(\theta)}{\mathrm{d}\theta^2}=-(x_2-x_1)\cos\theta-(y_2-y_1)\sin\theta \tag{75}$$

$$y'_{c_r}(\theta)=\frac{\mathrm{d}y_{c_r}(\theta)}{\mathrm{d}\theta}=-(x_2-x_1)\cos\theta-(y_2-y_1)\sin\theta - \frac{c_{w_{1_r}}(\theta)+c_{w_{2r}}(\theta)}{2y_4(\theta)} \tag{76}$$

$$y''_{c_r}(\theta)=\frac{\mathrm{d}^2y_{c_r}(\theta)}{\mathrm{d}\theta^2}=(x_2-x_1)\sin\theta-(y_2-y_1)\cos\theta + \frac{\left(c_{w_{1_r}}(\theta)+c_{w_{2_r}}(\theta)\right)^2}{4y_4(\theta)^3}-\frac{c_{w_{3_r}}(\theta)+c_{w_{4_r}}(\theta)}{2y_4(\theta)} \tag{77}$$

The first and second derivatives of the cam contour itself are:

$$y'_{c_r}\left(x_{c_r}\right)=\frac{y'_{c_r}\left(\theta\left(x_{c_r}\right)\right)}{x'_{c_r}\left(\theta\left(x_{c_r}\right)\right)}, \tag{78}$$

$$y''_{c_r}\left(x_{c_r}\right)=\frac{y''_{c_r}\left(\theta\left(x_{c_r}\right)\right)x'_{c_r}\left(\theta\left(x_{c_r}\right)\right)-y'_{c_r}\left(\theta\left(x_{c_r}\right)\right)x''_{c_r}\left(\theta\left(x_{c_r}\right)\right)}{x'_{c_r}\left(\theta\left(x_{c_r}\right)\right)^3}. \tag{79}$$

The radius of curvature equation for this specific regular wedge cam application can now be written as:

$$r_{rc}\left(x_c\right)=\frac{\left(1+y'_c\left(x_c\right)^2\right)^{3/2}}{y''_c\left(x_c\right)}, \tag{80}$$

and the initial conditions (at $x_{c0_r}=0$ and $\theta_0=0$) are:

$$y_{c_r}\left(x_{c0_r}\right)=y_{c0_r} \text{ and } y'_{c_r}\left(x_{c0_r}\right)=\frac{y'_{c_r}(\theta_0)}{x'_{c_r}(\theta_0)} \tag{81}$$

The nonlinear ODE application and associated validation procedures for the design configuration shown in Figure 4 are constructed from several specified/driving analysis variables: R_{wmax} = 4 in. (0.1016 m), R_{wmin} = 0.5 in. (0.0127 m), r = 2 in. (0.0508 m), C_{lrx} = 0.5 in. (0.0127 m), φ_o = 30˚, x_1 = 12.21 in. (0.3101 m) and y_1 = 11.14 in. (0.2829 m), and x_2 = 13.21 in. (0.3355 m) and y_2 = 18.29 in. (0.4646 m). Due to the complexity of this specific regular wedge cam theory, Simpson's rule (where $n=100$ and $m=100$) is utilized for approximating all integrals involved within this applied nonlinear ODE theory.

With experimentation, the plus/minus values for s_1 and s_2 were determined in alignment with Figure 5 below—as they affect the solution output due to the possibility of having more than one curve satisfying both the given radius of curvature function and the initial conditions (as seen within the three previous mathematical validation examples). The specific application to regular wedge cam design coupled with the chosen analysis variable parameters requires $s_1=+1$ and $s_2=+1$. This was determined by testing all solution numbers and comparing the ODE solution and its derivatives with the exact path equation and its derivatives.

Due to the use of Simpson's rule, the maximum error E_1 (between exact parametric and approximate ODE paths) is a 0.186% overestimate. The errors E_2 and E_3 (between exact parametric form and approximate ODE successive cam path derivatives) are all 0.000% underestimates.

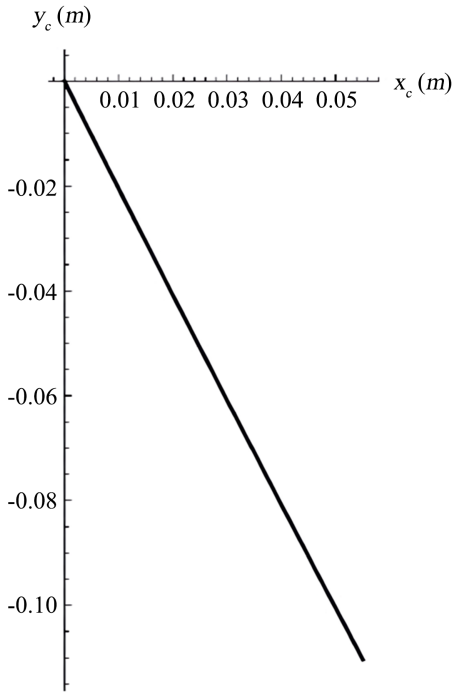

Figure 5. Regular wedge cam path.

Consequently, the nonlinear differential equation theory and Simpson's equations for both singular and nested integrals are validated. For other validation aspects regarding the parametric cam path equations, consult with research on the detailed derivation of generalized robust systems-based three-point self-centering motion theory in the design of regular and inverse wedge cams [11]. (**Table 1**)

Table 1. Validation of nonlinear ODE theory applied to regular wedge cam design.

Exact Values				Approximate Values				Percent Error Values		
θ	$y_{cr}(x_{cr})$	$y'_{cr}(x_{cr})$	$y''_{cr}(x_{cr})$	x_{cr}	$y_{cr}(x_{cr})$	$y'_{cr}(x_{cr})$	$y''_{cr}(x_{cr})$	E_1	E_2	E_3
(deg)	(m)	(-)	(1/m)	(m)	(m)	(-)	(1/m)	(%)	(%)	(%)
0	0.000	2.063	−2.633	0.000	0.000	2.063	−2.633	0.000	0.000	0.000
3	0.019	2.040	−2.283	0.009	0.019	2.040	−2.283	−0.170	0.000	0.000
6	0.038	2.020	−1.978	0.019	0.039	2.020	−1.978	−0.174	0.000	0.000
9	0.057	2.003	−1.761	0.028	0.057	2.003	−1.761	−0.176	0.000	0.000
12	0.075	1.987	−1.754	0.037	0.075	1.987	−1.754	−0.179	0.000	0.000
15	0.093	1.970	−2.335	0.046	0.093	1.970	−2.335	−0.182	0.000	0.000
18.06	0.110	1.940	−5.019	0.055	0.111	1.940	−5.019	−0.186	0.000	0.000

In closing, the rectangular form of the regular wedge cam contour utilized the derived nonlinear radius of curvature ODE solution which was performed as an exploratory effort as well as for its use in the optimization of related curvature and cam dynamic characteristics [12].

4. Conclusions with Limitations

The differential equation form of the radius of curvature is a fundamental concept in geometry that has widespread applications in engineering, physics, computer graphics, and robotics. Finding analytical solutions to these equations, particularly for complex curves, remains an area of active research. The theoretical insights into curvature, combined with computational methods, have enabled the practical application of curvature analysis in designing efficient structures, smooth animations, and precise robotic paths. As computational techniques continue to evolve, the ability to solve increasingly complex curvature-related problems will expand the range of applications and their precision.

As such, an exact fully generalized closed-form analytical curve function solution has been derived within a rectangular 2D Cartesian plane framework. Simpson's rule is then implemented into the mathematical nonlinear ODE theory to address complexities that may arise when analytically solving the required integrals for certain types of curvature functions. Additionally, the selection of the correct solution branch depends on the problem being considered. If the problem is of the pure mathematical type, then all solution branches are selected. If the problem is a real-world application, then one must choose a single solution that requires experimental evaluation.

In connection, this nonlinear ODE theory has been thoroughly validated within the application of three mathematical examples as well as within a more comprehensive application involving the motion of a self-centering regular wedge cam. To highlight, the regular wedge cam contour example was formulated using the rectangular form ODE solution, which relies on the radius of curvature and is useful for the optimization of related curvature, machine design, and cam dynamic characteristics. This allows an engineer to prescribe a radius of curvature, potentially as part of an objective function (if desired), for more effectively managing/balancing cam contact stresses and other related properties in context of deriving the required cam profile for producing the resulting self-centering motion.

Nevertheless, while empirical testing using cam profiles confirmed that the method exhibits the expected convergence behavior, it is important to note clamping accuracy regarding the self-centering wedge cam profile as error arises from the use of Simpson's rule in both single and nested integration steps. These effects are compounded by the square root terms in the solution formula, which can lead to numerical instability unless carefully validated.

Additional limitations arise from the structure of the nested Simpson's rule itself, which is not error-neutral and requires both suitable resolution and smooth

behavior to be effective. Furthermore, large values of n and m may introduce floating-point round-off risks, especially when compounded by square root and trigonometric operations. Mitigation strategies may include convergence testing, adaptive integration near critical regions, and verification of solution branches using known analytical benchmarks.

5. Future Research

Future research will involve the application of this work to inverse wedge cams as well as optimization of these cams when high curvature sensitivity minimization is required for providing deeper insight into design characteristics involving contact forces/stresses and associated machinery design as well as dynamics and related wear & fatigue. In conjunction, the specified analysis variables may be adjusted to examine the variation in error between multiple designs. The step size values used for Simpson's rule may also be adjusted to determine the speed of convergence and to examine the trade-off between error and computational efficiency.

Additional related research may involve applying the Gibbs-Appell method in conjunction with this specific nonlinear ODE theory for a better understanding of how forces and related vibrations affect real-world performance of these cam systems. Such exploration may pave way into physical prototypes of baseline vs. optimized concepts along with experimental testing coupled with studies into the nonlinear dynamic response of these cam types subjected to rapid load changes—particularly relevant in robotics applications—for analyzing how dynamic loads affect wear and longevity in relation to clamping accuracy.

Worth noting, in the case of curves described in a *parametric* 2D Cartesian plane framework, the differential equation for the radius of curvature takes a specific form (different from that presented within this research). Analytical methods for solving this form often rely on simplifying the parametric equations or applying numerical solutions when exact solutions are infeasible [13]. In connection, there are many practical applications where the need for computational methods has led to the development of algorithms that approximate the radius of curvature, especially in engineering and Computer-Aided Design (CAD) systems. Therefore, the generalized closed-form analytical solution to the aforementioned differential equation form of the radius of curvature may be shown as part of future research efforts.

Moreover, for multi-dimensional considerations, the analysis of curvature involves the concept of curvature tensors and the study of surfaces rather than simple curves. As the complexity of the systems being modeled increases, the need for advanced computational methods to handle these higher-dimensional curvatures becomes ever more critical [13]. Therefore, future research may be extended to curves described in polar, cylindrical, and spherical coordinate systems as well as multi-dimensional space in context of mathematical physics and related unified field theory research [14] [15].

Conflicts of Interest

The author has no conflicts of interest with this work.

References

[1] Goldstein, H. (1980) Classical Mechanics. 2nd Edition, Addison-Wesley.

[2] Timoshenko, S. and Goodier, J.N. (1970) Theory of Elasticity. 3rd Edition, McGraw-Hill. https://doi.org/10.1115/1.3408648

[3] Bartels, R.H., Beatty, J.C. and Barsky, B.A. (1987) An Introduction to Splines for Use in Computer Graphics and Geometric Modeling. Morgan Kaufmann Publishers.

[4] Latombe, J.C. (1991) Robot Motion Planning. Kluwer Academic Publishers. https://doi.org/10.1007/978-1-4615-4022-9

[5] Zienkiewicz, O.C., Taylor, R.L. and Zhu, J.Z. (2005) The Finite Element Method: Its Basis and Fundamentals. 6th Edition, Elsevier.

[6] Hibbler, R.C. (1974) Engineering Mechanics Dynamics. 7th Edition, Prentice Hall.

[7] Stewart, I. (2003) Galois Theory. 3rd Edition, Chapman & Hall/CRC.

[8] O'Neill, B. (2006) Elementary Differential Geometry. 2nd Edition, Academic Press.

[9] Gray, A. (1998) Modern Differential Geometry of Curves and Surfaces with Mathematica. 2nd Edition, CRC Press.

[10] Hughes-Hallett, D., Gleadon, A.M., *et al.* (1994) Calculus. John Wiley & Sons.

[11] Guillory, S.P., Barhorst, A.A., Lee, J., Gottumukkala, R., Raush, J.R. and Chambers, T.L. (2025) Generalized Robust Systems-Based Theoretical Kinematic Inverse/Regular Wedge Cam Theory for Three-Point Diametral Self-Centering Motion. *Journal of Applied Mathematics and Physics*, **13**, 729-796. https://doi.org/10.4236/jamp.2025.133040

[12] Shigley, J. and Uicker, J. (1995) Theory of Machines and Mechanisms. 2nd Edition, McGraw Hill.

[13] Do Carmo, M.P. (1976) Differential Geometry of Curves and Surfaces. Prentice-Hall.

[14] Haramein, N. and Rauscher, E.A. (2005) The Origin of Spin: A Consideration of Torque and Coriolis Forces in Einstein's Field Equations and Grand Unification Theory. In: Amoroso, R.L., Lehnrt, B. and Vigier, J.P., Eds., *Beyond the Standard Model: Searching for Unity in Physics*, The Noetic Press, 153-168.

[15] Dymnikov, A.D. (2013) The Matrix Theory of Mathematical Field and the Motion of Mathematical Points in N-Dimensional Metric Space. *Journal of Computational Methods in Sciences and Engineering*, **13**, 59-109. https://doi.org/10.3233/jcm-120454